Please cite as:
Schoenball, M., F. R. Walsh, M. Weingarten, and W. L. Ellsworth, 2017, How faults wake up: the Guthrie-Langston, Oklahoma earthquakes: The Leading Edge, *in press*.

How faults wake up: the Guthrie-Langston, Oklahoma earthquakes

Martin Schoenball, F. Rall Walsh*, Matthew Weingarten, William L. Ellsworth

Stanford University, Stanford, USA

* now at Decision Geomechanics LLC, San Francisco, USA

schoenball@stanford.edu

Abstract

Large-scale wastewater disposal has led to a fast-paced reawakening of faults in the Oklahoma/Kansas region. High resolution earthquake relocations show that the inventory of ancient basement faults in the study region differs from results of seismic surveys and geologic mapping focused on the sedimentary cover. We analyze the evolution of seismic activity in the Guthrie-Langston sequence in central Oklahoma in greater detail. Here, seismic activity has reactivated a network of at least 12 sub-vertical faults in an area less than 10 km across. Recorded activity began in late 2013 and peaked about 6 months later and includes two M4 earthquakes. These earthquakes characteristically occur at about 4 km depth below the top of the basement and do not reach the sedimentary cover. The sequence shows a radial growth pattern despite being no closer than 10 km to significant wastewater disposal activity. Hydrologic modeling suggests that activity initiated with a time lag of several years relative to early injection activity. Once initiated, earthquake interactions contribute to the propagation of seismicity along the reactivated faults. As a result, the spatio-temporal evolution of the seismicity mimics a diffusive pattern that is typically thought to be associated with injection activity. Analysis of the Fault Slip Potential shows that most faults are critically stressed in the contemporary stress field. Activity on some faults, for which we find low slip probability, suggest a significant contribution of geomechanical heterogeneities to the reawakening of these ancient basement faults.

Introduction

Since about 2009, the induced seismicity crisis in Oklahoma has produced a carpet of earthquakes that spans an area about 200 km across, stretching from Oklahoma City into southern Kansas. It is now generally accepted that the uptick of seismicity is caused by large-scale wastewater injection into the Arbuckle Group (Ellsworth, et al. 2015, Walsh and Zoback, 2015, Weingarten et al., 2015). Recent efforts to precisely relocate the activity – made possible through waveform data provided by private companies – show that the carpet of earthquakes is composed of discrete basement faults. This high-resolution image of the earthquakes provides unprecedented insights into the regional network of ancient basement faults in this previously quiescent intraplate region (Schoenball and Ellsworth, 2017).

In Figure 1 we summarize the current understanding of the link between wastewater and induced earthquakes in Oklahoma and Kansas. Wastewater is disposed into over 800 UIC class II wells. Wells are drilled into the Arbuckle Group and sometimes reached into the basement. Fluids are transported by trucks or through pipelines to disposal wells and injected into the high permeability Arbuckle Group. Addition of fluid creates a far-reaching plume of modestly elevated pore pressure (< 2 MPa) relative to the natural underpressured state of the Arbuckle. Permeable pathways from the Arbuckle into the basement raises the pressure in hydrologically connected basement faults, reducing their strength through the well-known effective stress relation (Raleigh et al., 1976). Earthquake sequences have been observed several 10s of kilometers away from large injectors elsewhere in Oklahoma (Keranen et al., 2014) where modeled effective stress changes at hypocentral depth are less than 0.5 MPa. Because of the many active disposal wells and the far-reaching pressure perturbation, it is generally impossible to associate induced sequences with injection activity of specific wells.

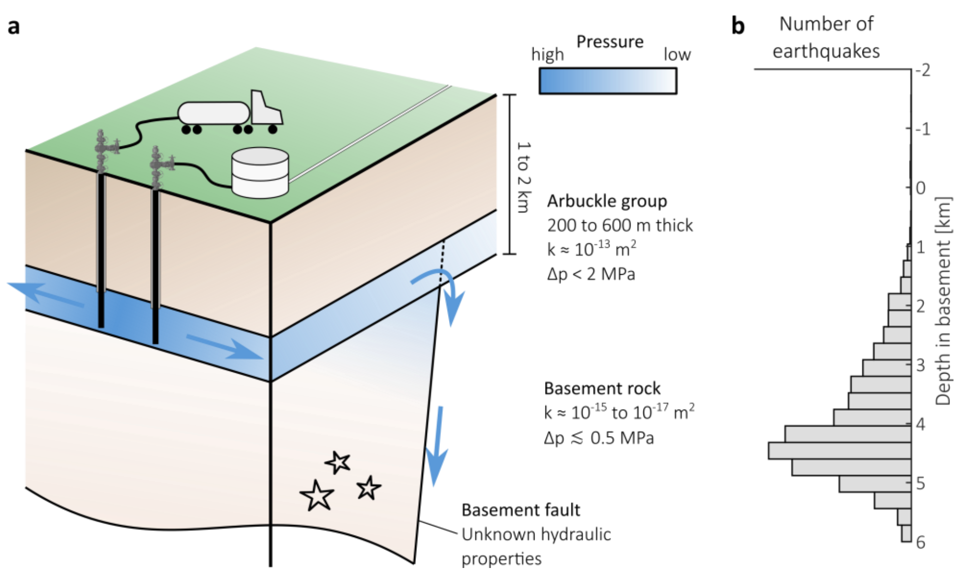

Figure 1: a) Conceptual model of induced seismicity in Oklahoma and southern Kansas. b) Observed focal depths of induced earthquakes in Oklahoma and southern Kansas relative to the base of the Arbuckle Group/top of basement (from Schoenball and Ellsworth, 2017).

Walsh and Zoback (2016) developed a probabilistic method to estimate the potential for fault reactivation based on geomechanical theory and Monte Carlo sampling of the relevant input parameter distributions. Based on known fault orientation and assumptions of the geomechanical conditions, they estimate the Fault Slip Potential (FSP) as a proxy for the probability of reactivating specific faults through injection operations.

Here we compare the fault structures resolved from precise earthquake relocations with the known inventory of basement faults. We model pore pressure changes in the Arbuckle Group and at hypocentral depths and test the FSP framework by applying it to these faults, and focus on a sequence of earthquakes between Guthrie and Langston, Oklahoma.

Regional fault network

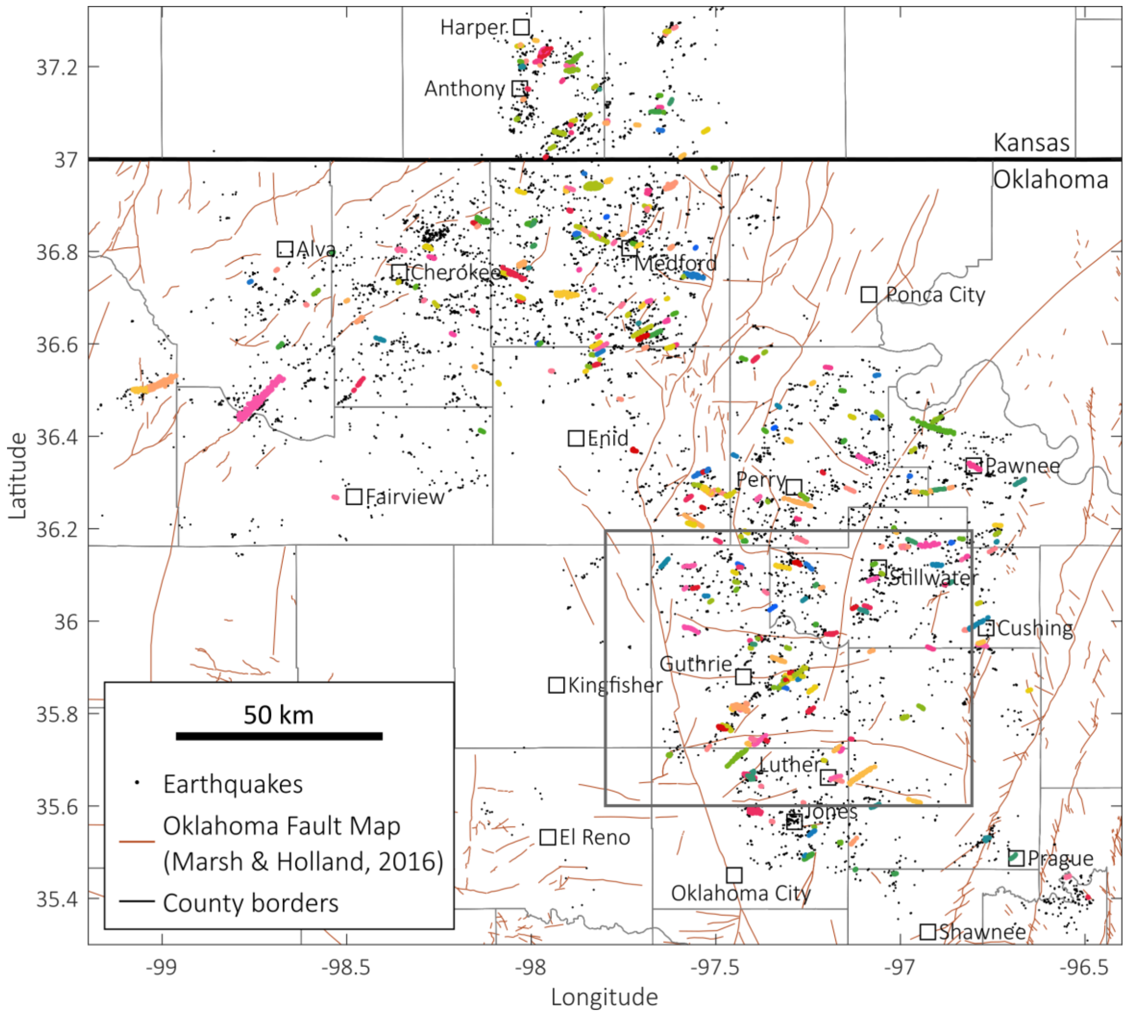

Figure 2: Map of relocated earthquakes in the Oklahoma and southern Kansas area. Earthquakes on interpreted faults are drawn in distinct colors. Brown lines are faults from Marsh & Holland (2016)*. The box shows the area of Figure 5.*

The refined earthquake relocations of Schoenball and Ellsworth (2017) are shown in Figure 2. Earthquakes cluster along tight lineations that we interpreted as individual basement faults. Both near-vertical and dipping structures are found, with most displaying strike-slip movement. Earthquakes generally occur in the basement, with the distribution of hypocentral depth peaking at 4 km below the top of basement (Figure 1b). Hypocenters in the sedimentary section are extremely rare.

Also shown in Figure 2 are the Oklahoma faults compiled by Marsh & Holland (2016). This map was compiled from interpretation of reflection seismic data and geologic mapping. Almost none of the earthquake sequences are associated with any of the mapped faults. Furthermore, we notice that the trends of mapped fault structures differ from the trends that are apparent from the earthquake locations. To further study the network of faults, we applied the DBSCAN algorithm (Ester et al., 1996) to objectively identify individual faults in the basement (Schoenball and Ellsworth, 2017). For each fault, we measure strike and dip using principal component analysis. More than 300 faults could be characterized in this way. We compare the strike of fault segments weighted by fault length with the mapped faults in Figure 3. For the Oklahoma Fault Map, we only consider fault segments that are at least partially within the area that has seen widespread seismicity in the last few years.

There is a clear difference in the dominant fault trends between both fault maps. In the Oklahoma Fault Map a large-scale NNE-SSW trend, related to the Nemaha Uplift and Midcontinent Rift System, predominates. This trend is absent in the faults illuminated by the earthquakes. Those faults show a clear pattern of conjugate faulting, that are favorably aligned for slip within the contemporary tectonic stress state. The predominant fault strikes from earthquake locations are in rough agreement with what would be expected from strike-slip faulting with the observed stress orientation (Figure 3). Strike directions that are associated with the Nemaha Uplift are stable in the contemporary stress field and, from a geomechanical perspective, are highly unlikely to reactivate regardless of the fluid pressure rise (Walsh and Zoback, 2016).

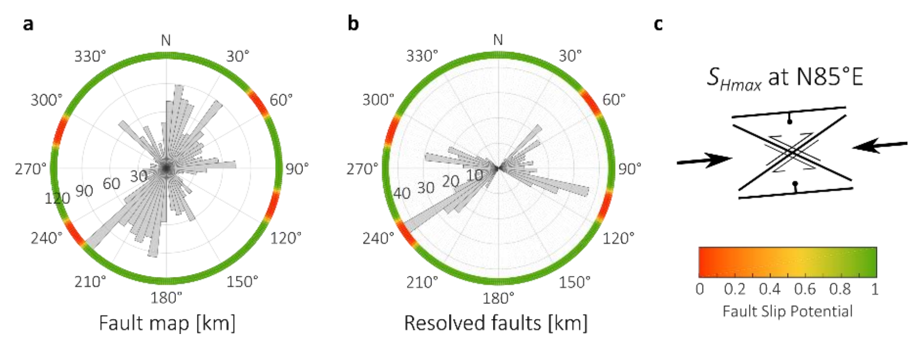

Figure 3: Comparison of fault strikes from (a) the Oklahoma Fault Map (Marsh and Holland, 2016) *and (b) resolved from earthquake hypocenters. The colors show the fault slip potential for vertical faults for comparison. (c) shows the orientation of critically stressed fault assuming S_{Hmax} oriented at N85°E* (Alt and Zoback, 2017).

Case study: The Guthrie-Langston sequence

The sequence of earthquakes that began in late 2013 between Guthrie and Langston in central Oklahoma is particularly rich in earthquakes (Benz et al., 2015) and resolved fault structures (Figure 4). We want to emphasize however, that many of the observations that we detail below are not specific to this sequence, but are found for other sequences in Oklahoma and Kansas as well.

We summarize the injection history and seismic activity in the Guthrie region in Figure 5. Minor wastewater injection about 10 km east of the Guthrie-Langston sequence occurred at least since 1997. Significant wastewater disposal with injection rates greater than 100,000 m^3 per month in single wells began in 2001. Injection in this area peaked between 2002 and 2007 and declined thereafter. Most of these wells are located along a N-S striking fault (Marsh and Holland, 2016) that potentially acted as a high permeable fluid conduit allowing for large injection volumes. North of Guthrie, large-scale injection started in 2012 and peaked in 2015. The monthly and cumulative injection volumes in the north never surpassed the volumes injected to the east.

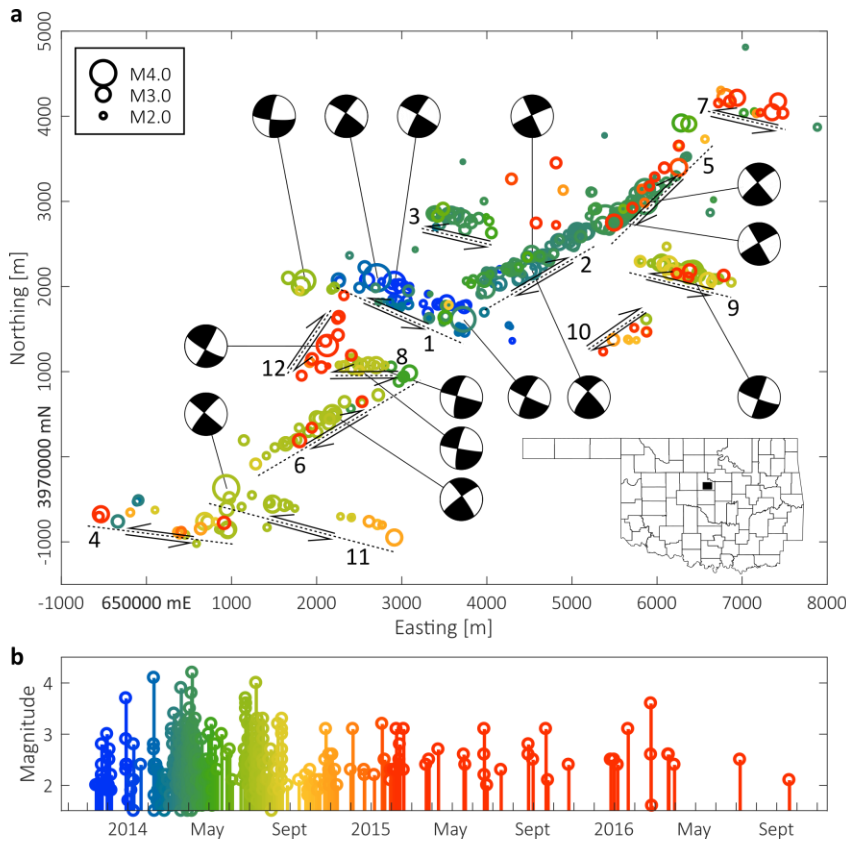

Figure 4: Evolution of the earthquake Guthrie-Langston sequence. (a) Map view with earthquakes colored by order of occurrence as in (b). Fault trends interpreted from the distribution of hypocenters are shown in dashed lines with the sense of slip indicated by arrows. Focal mechanisms are courtesy of Robert Herrmann (see Herrmann et al. 2011). *The inset in the bottom right shows the location of the map in the state of Oklahoma. (b) shows the temporal evolution of the sequence with colors the same as in (a).*

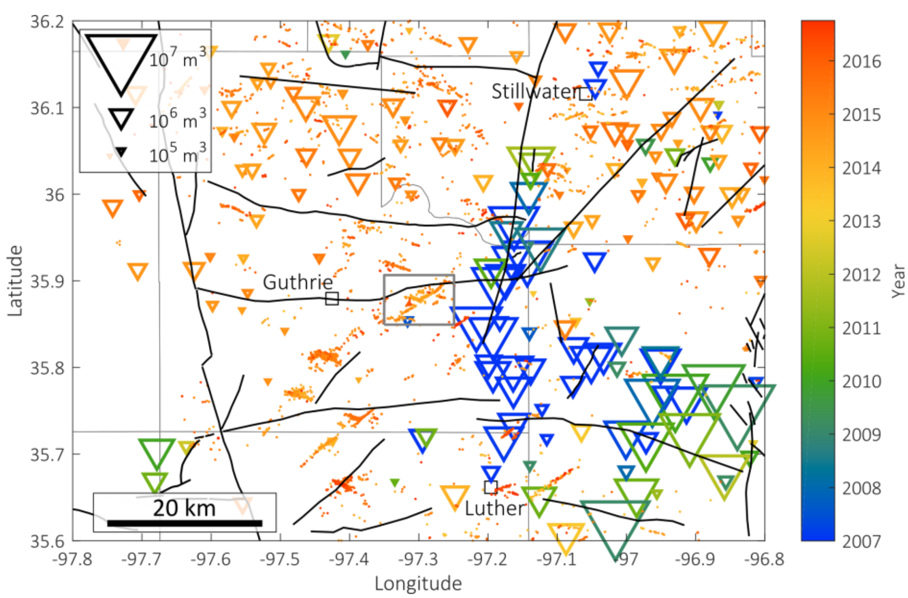

Figure 5: Injection wells and earthquakes around the Guthrie area. Earthquakes (dots) are colored by their time, injection wells (triangles) are sized by their cumulative injection volume between 1995 and 2016 and colored according to the period of highest injection (mean injection time weighted by volume). The box shows the area of Figure 4.

The first earthquakes were detected by the Oklahoma Geological Survey in late 2013 on a ESE striking fault (Fault 1) and activity propagated towards nearby Fault 2, to the northeast of Fault 1. Seismic activity reached a maximum rate in March and April 2014 when Faults 2 and 5 were in their most active phases (Figure 6). This was also the time when the two largest events of M4.2 and M4.1 occurred. Overall, 398 earthquakes were recorded through November 2016 when the catalog ends.

A delay from initiation to the highest rate of activity is observed in many sequences throughout Oklahoma (Schoenball and Ellsworth, 2017). Pre-shock activity typically builds over the course of a sequence, but sequences never start with the largest event. This pattern is distinctly different from bursts of natural seismicity, where we typically observe the mainshock preceded by only a small number of foreshocks, if any. Hence, the seismicity rate is highest early-on in a sequence. The occurrence pattern of the induced earthquakes suggests that these sequences are initiated by different processes. The rise of activity to its peak can be interpreted as a probing of the criticality of faults by the anthropogenic stressing (Dempsey and Suckale, 2016). More and larger asperities of faults activate as forcing continues.

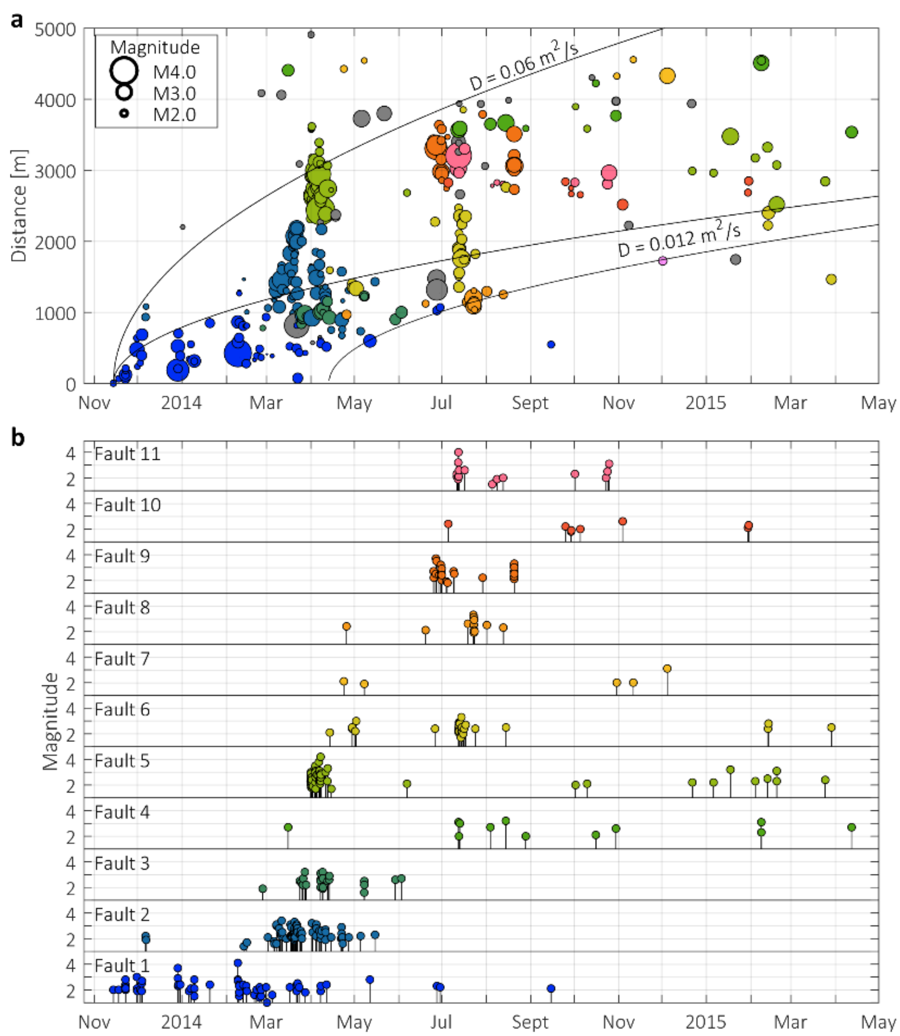

Figure 6: (a) Spatio-temporal evolution of the Guthrie-Langston sequence. Events are grouped by a distinct color for each fault. (b) shows the magnitude and timing of earthquakes grouped for each fault. Fault 12 is not shown because only one event falls in the time window shown.

A remarkable feature of the Guthrie-Langston sequence is the radial growth readily visible in Figure 4. The sequence eventually spreads northeast and southwest by 4 km involving 12 distinct faults that activate in succession. Later activity on two faults to the north and to the ESE (Figure 5) may be interpreted as a continuation of the radial growth pattern to even greater distances.

The radial expansion of the sequence is surprising since the closest class II injection well is 3 km from the geometric origin of the sequence and this well only injected a small volume and mostly before 2009 (Figure 5). This contradicts the classic view that pressure diffusion away from an injection well is reflected in the spatio-temporal growth pattern of a seismicity cloud (Shapiro et al., 1997). Rather, the growth pattern we observe in the Guthrie-Langston sequence may result from interactions of earthquakes through static stress transfer due to the displacement of each event. As earthquakes occur, neighboring faults are loaded by the displacements and may also activate (Figure 4a). The clear radial migration pattern does not seem to originate from any injection wells. Instead, we infer that other structures act as fluid conduit from the Arbuckle to the fault that initially reactivated (Figure 1). The sequence then grew, driven by the stress or pressure perturbation originating at the intersection between the first fault and the fluid conduit.

Pore pressure modeling of all Arbuckle injection wells within 30 kilometers of the Langston-Guthrie sequence shows how changes in pore pressure are manifested in the reservoir formation (Arbuckle Group) and the underlying basement fault (Figure 7). The modeling follows the conceptual framework shown in Figure 1, after Weingarten and Zoback (2016) and Walsh and Zoback (2015). Permeability in the Arbuckle Group is represented by a spatially heterogeneous, log-normal distribution in 100 stochastic realizations (mean $k = 10^{-13\pm0.7}$ m^2). The Arbuckle Group overlies a low-permeability, intact crystalline basement ($k = 10^{-17}$ m^2) with a permeable fault zone representing the Guthrie-Langston complex ($k = 10^{-15}$ m^2).

Modeled pressure rise in the Arbuckle Group at the location of the Guthrie-Langston sequence reached between ≈ 0.5 – 0.8 MPa, peaking in 2008 and slowly falling until about 2014 when it began to rise again due to injection activity to the north. Modeled pressure changes at hypocentral depth, however, steadily rose by ≈ 0.2 – 0.3 MPa since injection began in about 2002 and were still rising at the end of the simulation. The current modeled rate of pressure increase at hypocentral depth is less than previously observed during 2007 – 2009.

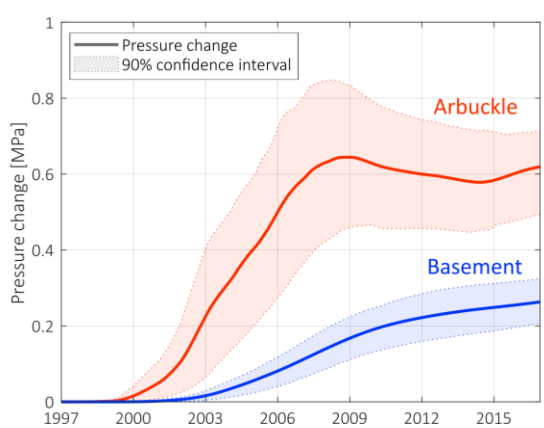

Figure 7: Modeled pore pressure changes in the Arbuckle Group and at 4.5 km below the top of basement at the location of the Fault 1 in the Guthrie-Langston sequence. The shaded pressure interval is obtained from sampling 100 realizations of log-normal stochastic permeability distributions in the Arbuckle Group.

One important result of the modeling shows how the permeability contrast between the Arbuckle Group and the permeable basement delays the onset of pressure propagation to hypocentral depths. Modeled pressures peaked in 2008 in the Arbuckle Group, without any observed seismicity in this sequence until late 2013. Pressure diffusion to hypocentral depths takes years to exceed a critical pressure to induce slip. Furthermore, the modeling indicates that measured pressure changes in the Arbuckle Group alone may be insufficient to adequately characterize pressure changes at hypocentral depths, and thus, induced seismic hazard into the future. Therefore, a combination of measured pressures and calibrated models are needed to adequately characterize and manage future induced seismic hazard (Yeck et al., 2016).

In Figure 6a we plot the growth of the sequence as the distance from the first earthquake, separately coloring each fault. We see that the initial activity on Fault 1 can be modeled by a diffusive process with D = 0.012 m^2/s. Later, activity jumps to other faults and also ahead of the initial triggering front. In order to fit all activity into a single diffusive process, D has to be of the order of 0.06 m^2/s. Another possible interpretation is that every fault spawns its own sub-sequence with a different diffusivity as can be observed in the r-t plot in Figure 6a.

We also observe differences in the temporal behavior of activity on each fault. Once activated, some faults show continuous activity (e.g. Fault 1 has activity over about 6 months), while others have short-lived bursts (e.g. fault 5 was active for just over two weeks). This suggests that activity on some faults is dominated by slow processes such as fluid diffusion, and activity on others is dominated by fast processes such as stress transfer from one rupture to the next. It is particularly noteworthy that none of the individual faults activate with their largest event. Instead, the observed largest magnitudes tend to increase as more events are produced (Figure 6b). This is in agreement with the statistical model of van der Elst et al. (2016) where each earthquake magnitude is an independent sample of the local magnitude-frequency distribution.

The complex spatio-temporal behavior is evidence for several processes at play in the development of induced earthquake sequences. We therefore regard estimates of diffusivity based on the spatio-temporal envelope of seismicity to infer the seismogenic diffusivity (Talwani et al., 2007) – a convolution of the hydraulic diffusivity, stress redistribution and processes that sample the heterogeneity and the criticality of the tectonic stress field.

After about five months, activity on Fault 1 declined as it migrated away from its origin. As a result, we see a zone of quiescence spreading from the origin (Figure 6a). The envelope of this spreading zone of quiescence can also be approximated by a diffusion process with D = 0.012 m^2/s. This back front (Parotidis, 2004) seems to exist also for later activity on other faults. The existence of a back front suggests that seismicity is driven by a stress perturbation that relaxes after it sweeps over the faults. The coincidence of the diffusivity obtained for the initial activity on Fault 1 and the back front suggests both represent the same process. The continuous activity on Fault 1 and the absence of activity bursts indicates that earthquake interactions are less important for driving seismicity on this fault. From these observations, we conclude that the diffusivity observed for the triggering and back fronts is indeed the hydraulic diffusivity of the fault system.

Retrospective estimations of fault slip potential

The identified fault structures can be used to test the FSP approach of Walsh and Zoback (2016). But first we must assess the precision of the earthquake hypocenters from which the fault structures were derived. Earthquakes can generally be located more precisely in latitude and longitude than in depth. For the relocated catalog, the vertical precision is about a factor 5 to 10 less than the horizontal. To get accurate estimates of an earthquake's depth, we require stations that are close to the epicenter, typically closer than one focal depth. For the Guthrie-Langston sequence, the closest stations are between 5 and 15 km away from the events and seismicity is about 6 km deep. This is not sufficient to resolve the vertical structure in detail. As a result, the dip angles of resolved faults may be systematically biased.

Moment tensor solutions for the larger events provide an independent constraint of fault dip. Here we use moment tensor solutions determined by St. Louis University (see Herrmann et al. (2011) for details on their methods). Generally, the strike and, with some exceptions, the dip of faults determined from the hypocenters is in good agreement with one of the nodal planes of moment tensor solutions obtained from waveform modeling (Figure 4). In some cases, the lack of close-by stations provides insufficient coverage to resolve the fault dip. As a result, the resolved fault planes get vertically compressed in the relative relocation step and derived dip angles are unrealistically low. The most obvious example is Fault 1 which has a very well-defined fault plane. The dip resolved from earthquake hypocenters is an unreasonably low 33°. Moment tensors of the two largest events associated with this structure have dips of 80° and 85°. To reconcile this discrepancy, we estimate the minimal along-dip extent of fault reactivation as the rupture length of largest events. We assume a roughly circular rupture area of 1 km across for this M4.2 event. The fault is activated along about 1700 m of strike and all hypocenters associated with this fault are distributed over about 270 m along the dip direction. We estimate the lower bound on the dip using these dimensions to be about 75°. This is in rough agreement with the moment tensors.

The distribution of seismometers provides suitable azimuthal coverage to precisely constrain the epicenters of earthquakes and we do not expect a systematic error in the strike of faults. Uncertainties of the resolved fault strikes were estimated from bootstrap resampling of hypocenters used for the principal component analysis.

Estimation of the Fault Slip Potential requires several steps (Walsh and Zoback, 2016). First, the local stress field has to be characterized. This can be done using stress determinations from borehole data and inversion of focal mechanisms (Zoback et al., 2003, Hardebeck and Michael, 2006). Distributions of the stress measurements can be obtained from bootstrap resampling of inverted focal mechanisms and from statistical analysis of borehole data (Schoenball and Davatzes, 2017). Furthermore, distributions of the coefficient of friction and initial pore pressure are assumed (Nelson et al., 2015, Carpenter et al., 2016). Using Mohr-Coulomb faulting theory and Monte Carlo sampling of the input parameter distributions, the probability of a fault slipping under a given pressure change is estimated (Walsh and Zoback, 2016).

The state of stress on each fault is both heterogeneous and uncertain. While most geomechanical modeling software model stress variability but not uncertainty, FSP models uncertainty but not variability. FSP assumes that each mechanical model is spatially uniform and stress is linearly increasing with depth. Uncertainty is modeled by assuming uniform distributions which are taken as the 2nd and

98th percentile of distributions (of varying shape) in Walsh and Zoback (2016). The result of FSP is a distribution of pore pressure to slip on each fault.

In Figure 8 we summarize the estimated FSP for three different assumptions about the orientation of interpreted faults within the same uncertain stress field. In the first case, we calculate FSP using the strike and dip as estimated from the relocated earthquake hypocenters with no uncertainty in either value. Only 6 out of 12 faults have a FSP larger than 0.5 in this case, and 4 have no potential to slip if 2 MPa is added to them. However, as discussed above, we are not confident about the fault dip angles. We are, however, confident about the resolved strikes. Therefore, in column 2 we compute FSP for the resolved strike and assume a dip of 85°±5°. Now, 7 out of 12 faults have a FSP of larger than 0.5 and all have at least 4% slip potential. In the third case, we also allow the strike to vary as a uniform distribution within its 2-σ interval. 7 out of 12 faults still have FSP > 0.5, but slip potentials have generally increased. This analysis demonstrates the importance that the fault orientation relative to the stress field has on estimates of FSP. Discrepancies as small as 10° or less can have a strong impact on FSP.

Fault 12 is the last fault to be activated during this sequence and the activated fault with the lowest FSP. It is misoriented by about 20° from the optimal strike for failure if the maximum horizontal stress is trending at 82°. The fault orientation is interpreted based on hypocenters of 10 events. The focal mechanism of the largest M3.6 event has a strike of 29° in close agreement with the interpreted fault strike of 35°. We therefore trust this fault orientation. This suggests that at scales of smaller faults heterogeneity of stress might play a significant role. The late activation of the fault and its proximity to earlier active faults suggests that previous activity on nearby faults may contribute to changing the state of stress on this fault such that it became reactivated. However, it is unlikely that static stress transfer rotated the stress state enough to enable Fault 12 to slip. Instead, local heterogeneity of the stress field may have caused this fault to slip under moderate stress perturbations. Alt and Zoback (2017) found that the stress orientation is consistent on a large scale in the Oklahoma region. However, stress rotations of 20° or more are frequently observed locally in borehole data. Such rotations can be explained by slip on faults and reflect the heterogeneity of the state of stress (Barton and Zoback, 1994, Sahara et al., 2014, Schoenball and Davatzes, 2017).

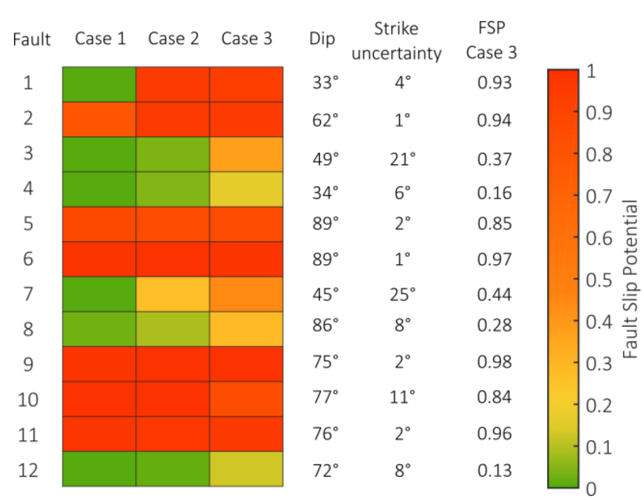

Figure 8: Fault Slip Potential after Walsh & Zoback (2016) *for faults derived from hypocenter locations for different assumptions of the accuracy of the resolved strike and dip. Case 1 assumes strike and dip as resolved from earthquake hypocenters, Case 2 assumes dip of 85°±5° and strike as resolved from earthquake hypocenters and Case 3 assumes dip of 85°±5° and strike and its 2σ-error.*

In Figure 9 we summarize the influence of each parameter of the FSP analysis on fault number 1 under case 3, with strike of 115°±4° and dip of 85°±5°. This is done by calculating the pore pressure to slip with each parameter at the center, lower and upper bound of its distribution. Those parameters that provide the largest variability in answers are ranked at the top. For this fault, it is readily apparent that the pressure to slip is most sensitive to the frictional properties of the fault and the magnitude of the stress state (as represented by the reference friction). These are followed in importance by the strike of the fault relative to the trend of S_{Hmax}. It is not surprising that the pressure to slip is not sensitive to the vertical stress because in a strike-slip faulting regime, it is the intermediate principal stress. Similarly, the uncertainty of the relative stress magnitudes, described by the a_ϕ parameter, does not play a significant role within its uncertainty. This can be used to inform prioritization of which parameters should be better constrained to decrease uncertainty.

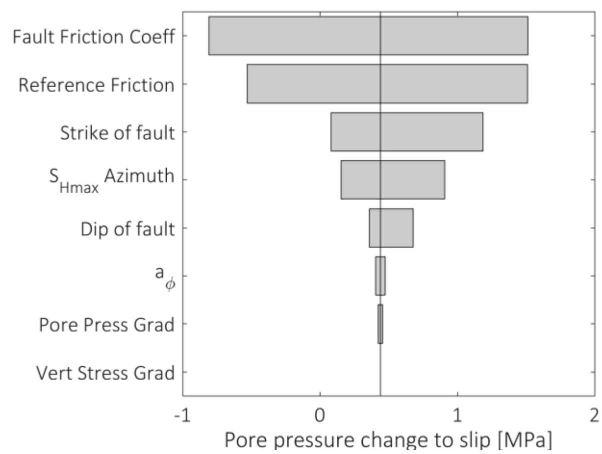

Figure 9: Tornado diagram summarizing the impact of variations of the input parameters on the Fault Slip Potential for fault 1.

Conclusions

Refined earthquake locations provide an image of the reawakened fault structures at high resolution enabling us to study their evolution in detail. Sequences of induced earthquakes typically grow to larger magnitudes after they initiate with minor activity. We do not typically see a mainshock-aftershock pattern without any prior activity. Improved monitoring can help to anticipate potentially damaging sequences. Reducing injection activity typically reduces the earthquake activity and lessens the probability for large magnitude events to occur (Langenbruch and Zoback, 2016).

The Guthrie-Langston sequence occurred with a large temporal and spatial separation from the nearest injection activity. Large scale injection east of the sequence does not show an immediate temporal correlation with the occurrence of these earthquakes. There is a stronger temporal correlation with the onset of large-scale injection activity about 15 km north of the sequence. However, stochastic pore pressure modeling indicates both injection areas contributed to the delayed pressure diffusion to depth. Modeled pressures in the Arbuckle Group peaked in 2008 and have slowly declined, but pressure at hypocentral depths in the Guthrie-Langston sequence has steadily increased through the end of 2016. Due to the large number of disposal wells and large distances between injection sites and seismicity sequences, it remains difficult to associate activity in isolated sequences to particular wells.

Previously, the correlation of injection activity and earthquake occurrence in space and time has been used as a strong argument to identify man-made sequences (Davis and Frohlich, 1993). We have shown that the Guthrie-Langston sequence grows in a radial pattern, reminiscent of a radial diffusion process originating at an injection well (Shapiro et al., 1997). However, there is no injection well near the sequence origin and different processes must be at play to propagate the seismicity such as static stress transfer.

Analysis of the Fault Slip Potential for the reactivated faults has shown significant probability for slip for most reactivated faults. Low FSP values for few faults may indicate to the role largely unknown heterogeneities of the geomechanical conditions such as state of stress and friction play. FSP analysis can only be useful if we have a good understanding of the faults in the area of interest and their geomechanical state. Potential pitfalls in its application include large uncertainties (such as sliding friction, cf. Figure 9), and incomplete sampling of strike-slip basement faults through seismic imaging in quiescent sediments but not in the seismogenic basement. Unfortunately, it remains a geophysical challenge to image ancient sub-vertical faults in igneous basement through active seismic surveys.

Acknowledgements

M.S. acknowledges support by the Alexander von Humboldt Foundation. All authors were supported by the Stanford Center for Induced and Triggered Seismicity.

References

Alt, R. C., and M. D. Zoback, 2017, In Situ Stress and Active Faulting in Oklahoma. Bulletin of the Seismological Society of America, **107**, 216–228.

Barton, C. A., and M. D. Zoback, 1994, Stress perturbations associated with active faults penetrated by boreholes: Possible evidence for near-complete stress drop and a new technique for stress magnitude measurement. Journal of Geophysical Research, **99**, 9373.

Benz, H. M., N. D. McMahon, R. C. Aster, D. E. McNamara, and D. B. Harris, 2015, Hundreds of Earthquakes per Day: The 2014 Guthrie, Oklahoma, Earthquake Sequence. Seismological Research Letters, **86**, 1318–1325.

Carpenter, B., C. Morgan, D. Lockner, and Z. Reches, 2016, Strength and Stability of Oklahoma Basement Rock: Preliminary Observations from Experiments at In-situ Conditions: American Geophysical Union, Fall Meeting 2016. San Franscisco, California, USA.

Davis, S. D., and C. Frohlich, 1993, Did (Or Will) Fluid Injection Cause Earthquakes? - Criteria for a Rational Assessment: Seismological Research Letters, **64**, 207–224.

Dempsey, D., and J. Suckale, 2016, Collective properties of injection-induced earthquake sequences: 1. Model description and directivity bias: Journal of Geophysical Research: Solid Earth, **121**, 3609–3637.

Ellsworth, W. L., A. L. Llenos, A. F. McGarr, A. J. Michael, J. L. Rubinstein, C. S. Mueller, M. D. Petersen, and E. Calais, 2015, Increasing seismicity in the U. S. midcontinent: Implications for earthquake hazard. The Leading Edge, **34**, 618–626.

van der Elst, N. J., M. T. Page, D. A. Weiser, T. H. W. Goebel, and S. M. Hosseini, 2016, Induced earthquake magnitudes are as large as (statistically) expected: Journal of Geophysical Research: Solid Earth, **121**, 4575–4590.

Ester, M., H.-P. Kriegel, J. Sander, and X. Xu, 1996, A Density-Based Algorithm for Discovering Clusters in Large Spatial Databases with Noise: Page Proc. 2nd int. Conf. on Knowledge Discovery and Data

Mining (KDD ‘96). AAAI Press, Portland, Oregon.

Hardebeck, J. L., and A. J. Michael, 2006, Damped regional-scale stress inversions: Methodology and examples for southern California and the Coalinga aftershock sequence: Journal of Geophysical Research, **111**, B11310.

Herrmann, R. B., H. Benz, and C. J. Ammon, 2011, Monitoring the Earthquake Source Process in North America: Bulletin of the Seismological Society of America, **101**, 2609–2625.

Keranen, K. M., M. Weingarten, G. A. Abers, B. A. Bekins, and S. Ge, 2014, Sharp increase in central Oklahoma seismicity since 2008 induced by massive wastewater injection: Science, **345**, 448–451.

Langenbruch, C., and M. D. Zoback. 2016. How will induced seismicity in Oklahoma respond to decreased saltwater injection rates? Science Advances **2**:e1601542.

Marsh, S., and A. A. Holland, 2016, Comprehensive Fault Database and Interpretive Fault Map of Oklahoma: Open-File Report, OF2-2016, Oklahoma Geological Survey, Norman.

Nelson, P. H., N. J. Gianoutsos, and R. M. Drake II, 2015, Underpressure in Mesozoic and Paleozoic rock units in the Midcontinent of the United States: AAPG Bulletin, **99**, 1861–1892.

Parotidis, M, 2004, A statistical model for the seismicity rate of fluid-injection-induced earthquakes: Geophysical Research Letters, **31**, L17609.

Raleigh, C. B., J. H. Healy, and J. D. Bredehoeft, 1976, An Experiment in Earthquake Control at Rangely, Colorado: Science, **191**, 1230–1237.

Sahara, D. P., M. Schoenball, T. Kohl, and B. I. R. Müller, 2014, Impact of fracture networks on borehole breakout heterogeneities in crystalline rock: International Journal of Rock Mechanics and Mining Sciences, **71**, 301–309.

Schoenball, M., and N. C. Davatzes, 2017, Quantifying the heterogeneity of the tectonic stress field using borehole data: Journal of Geophysical Research: Solid Earth, **122**, 6737–6756.

Schoenball, M., and W. L. Ellsworth, 2017, A systematic assessment of the spatio-temporal evolution of fault activation through induced seismicity in Oklahoma and southern Kansas: Journal of Geophysical Research: Solid Earth, in press, doi:10.1002/2017JB014850.

Schoenball, M., and W. L. Ellsworth, 2017, Waveform-Relocated Earthquake Catalog for Oklahoma and Southern Kansas Illuminates the Regional Fault Network: Seismological Research Letters, **88**, 1252–1258.

Shapiro, S. A., E. Huenges, and G. Borm, 1997, Estimating the crust permeability from fluid-injection-induced seismic emission at the KTB site: Geophysical Journal International, **131**, F15–F18.

Talwani, P., L. Chen, and K. Gahalaut, 2007, Seismogenic permeability, ks: Journal of Geophysical Research, **112**, B07309.

Walsh, F. R., and M. D. Zoback, 2015, Oklahoma’s recent earthquakes and saltwater disposal: Science Advances, **1**, e1500195.

Walsh, F. R., and M. D. Zoback, 2016, Probabilistic assessment of potential fault slip related to injection-induced earthquakes: Application to north-central Oklahoma, USA: Geology, **44,** 991–994.

Weingarten, M., S. Ge, J. W. Godt, B. A. Bekins, and J. L. Rubinstein, 2015, High-rate injection is associated with the increase in U.S. mid-continent seismicity: Science, **348**, 1336–1340.

Weingarten, M. and Zoback, M.D., 2016, Are we past peak pressure in Oklahoma? A hydrogeologic evaluation of reduced saltwater injection rates on induced seismicity: American Geophysical Union, Fall General Assembly 2016, abstract #S43C-2870.

Yeck, W.L., Sheehan, A.F., Benz, H.M., Weingarten, M. and Nakai, J., 2016, Rapid Response, Monitoring, and Mitigation of Induced Seismicity near Greeley, Colorado: Seismological Research Letters, **87**, 837-847.

Zoback, M. D., C. A. Barton, M. Brudy, D. A. Castillo, T. Finkbeiner, B. R. Grollimund, D. B. Moos, P. Peška, C. D. Ward, and D. J. Wiprut, 2003, Determination of stress orientation and magnitude in deep wells: International Journal of Rock Mechanics and Mining Sciences, **40**, 1049–1076.